JOURNAL OF APPLIED POLYMER SCIENCE VOL. 20, 217–242 (1976)

# Isothermal Rupture Characteristics of a Plasticized Poly(vinyl Chloride) in the Glass–Rubber Transition Zone

E. M. SMOLEY, *Armstrong Cork Company, Research and Development Center, Lancaster, Pennsylvania 17604*

## Synopsis

Constant strain-rate uniaxial extension tests to rupture were performed at 23°C on a plasticized poly(vinyl chloride) (PVC) in the glass-to-rubber transition zone, $T_g = -18$°C, where experimental failure time $t_f$ is equal to or greater than material relaxation time $\tau$. Range of strain rates is from $1.8 \times 10^{-4}$ to $1.8 \times 10^{-1}$ $sec^{-1}$. The rupture characteristics in stress/strain time space are analyzed on the three coordinate planes. Time and deformation separability are examined in a nonlinear-constitutive relation. Rupture data on the coordinate planes are described by the Bueche-Halpin theory in which time effects are considered through a small-deformation viscoelastic property. Fracture surface morphology and separation processes in the crack tip are related to rupture characteristics.

## INTRODUCTION

For amorphous polymer systems, considerable attention has been given to relating macroscopic fracture or rupture characteristics to viscoelasticity and molecular network properties. Reviews are given by Smith,[1] Eirich et al.,[2] Landel et al.,[3] and Berry.[4] On the other hand, there is a growing body of information[4–7] on fracture or rupture surface morphologies and the separation mechanisms at intrinsic or preformed crack tips. A need exists to correlate these two approaches because a knowledge of crack tip conditions is required not only to interpret ultimate macroscopic properties, but also to develop rupture or fracture theories. Such a correlation is attempted in the present inquiry using a plasticized PVC composition in the glass-to-rubber transition zone. Similar approaches have been published by Manson and Hertzberg[8] and by Brown et al.[9]

## EXPERIMENTAL

### Material Composition

Material ingredients consist of a PVC resin, Firestone's FPC 9282; a plasticizer, di-2-ethyl hexyl phthalate (DOP); and a dibutyltin thermal stabilizer. Levels on the plasticizer and stabilizer are 40 phr and 2 phr, respectively. The $\bar{M}_w$ for the PVC resin is $5.51 \times 10^4$, and the $\bar{M}_n$ is $2.91 \times 10^4$.

## Material Process Conditions

Ingredients were mixed using dry-blending techniques in a Henschel mixer. Consolidation and fusion of the mix were carried out in a cavity mold. Six min were allowed for the mold containing the mix to preheat from room temperature to 177°C (350°F). The mold was then pressurized and maintained at 177°C for an additional 6 min. At the end of this time, the heat was discontinued and a final 6 min period was allowed for the mold to cool to room temperature, the cavity pressure still being maintained.

The material was fabricated in sheets 9.0 in. (22.9 cm) × 9.0 in. (22.9 cm) × 0.10 in. (0.254 cm). Only fully consolidated material was selected for test. Full consolidation was indicated by equality between the experimentally measured density and the density calculated from the weighted sum of specific volumes for the ingredients. Calculated density was 1.247 g/cm$^2$.

## Microstructure

The precise microstructure of PVC is speculative. Tobolsky[10] et al. point out that it appears to have a semicrystalline structure, the crystallites being small enough to act as crosslinks. More recently, according to Rehage,[11] the crystallites are randomly oriented crystal nuclei that are imbedded in and crosslink an amorphous polymer microstructure. Tobolsky[10] also noted that the crystallites in PVC remained stable under the action of a DOP plasticizer.

## Apparatus

Concentric ring test specimens 1.188-in. (3.02 cm) I.D. × 1.313-in. (3.34 cm) O.D. × 0.1 in. (0.254 cm) thickness were die cut from a sheet of the material. Dimensions of each ring were measured under an optical microscope at the test temperature, 23°C.

Ring specimens were installed over two 0.40-in. (1.02 cm)-diameter pins (Fig. 1) which were separated at a constant extension rate in an Instron tensile machine. These pins were coated with a film of silicone grease to lower sliding friction between the pin and specimen during extension.

Smith[12,13] found that the O.D./I.D. ratio of a ring specimen should be 1.1 or less, in order to minimize the stress difference between the O.D. and I.D. For the present inquiry, the ratio is 1.1.

Experiments[12,13] have also indicated that stress/strain curves for the concentric ring specimens were in good agreement with those obtained on a conventional dogbone tensile geometry, providing the strain in the ring was based on its unstretched inner diameter. Thus, ring strain is given by

$$\epsilon = \frac{2\Delta l}{\pi D_i} \tag{1}$$

where $\Delta l$ is the pin travel, $D_i$ is the inside diameter (unstretched) of the ring, and $\epsilon$ is the nominal or engineering strain, that is, the change in specimen length divided by its original length. Nominal or average ring stress was calculated by dividing the retractive force $F$, (Fig. 1) by twice the cross-sectional area of an underformed ring. It has been shown[12,13] that, given the cross-

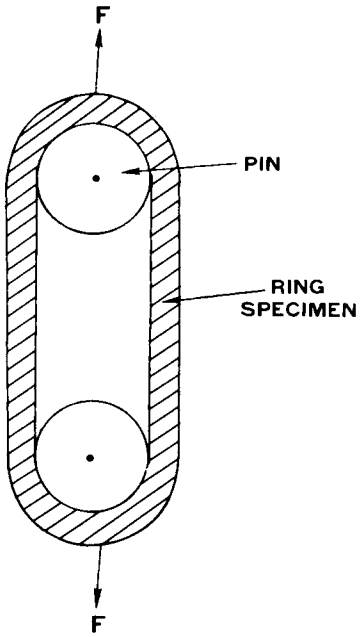


Fig. 1. Loading configuration for the concentric ring specimen in tension.

head speed, the corresponding strain rate can be calculated from eq. (1); moreover, the strain rate so calculated is constant until rupture.

Strain rate in the present study ranged from $1.8 \times 10^{-1}$ to $1.8 \times 10^{-4}$ $sec^{-1}$. Over this range, rupture did not preferentially occur where the load pin makes contact with the ring specimen. Test temperature was 23° ± 1.0°C, and the relative humidity was 50% ± 2%.

Microscopy was carried out using a Jeolco JSM-U3 scanning electron microscope and a Leitz research microscope Ortholux-Pol using transmitted light. The latter was used to view the dynamics of the separation processes in the crack tip.

## RESULTS AND DISCUSSION

### Stress–Strain Data at Constant Strain Rate

Figure 2 shows the engineering or nominal stress/strain curves for ten constant strain rates between $1.8 \times 10^{-4}$ to $1.8 \times 10^{-1}$ $sec.^{-1}$. Each curve is an average of three. The rupture stress $\sigma_f$ and strain $\epsilon_f$ are represented by the terminal point on each curve, and the greatest data scatter around each point is 5% for the stress and 7% for the strain with averages of 2.4% and 3.3%, respectively. Time to failure $t_f$ for the highest strain rate is 11.9 sec, and for the lowest strain rate, 7450 sec. Note in particular the change or transition in the rupture behavior at a strain rate of $1.8 \times 10^{-2}$ $sec^{-1}$. This is an interesting change in the ultimate properties of the plasticized PVC, and later it will be the subject of analysis and interpretation. It is assumed that the curves in Figure 2 were obtained under isothermal conditions.

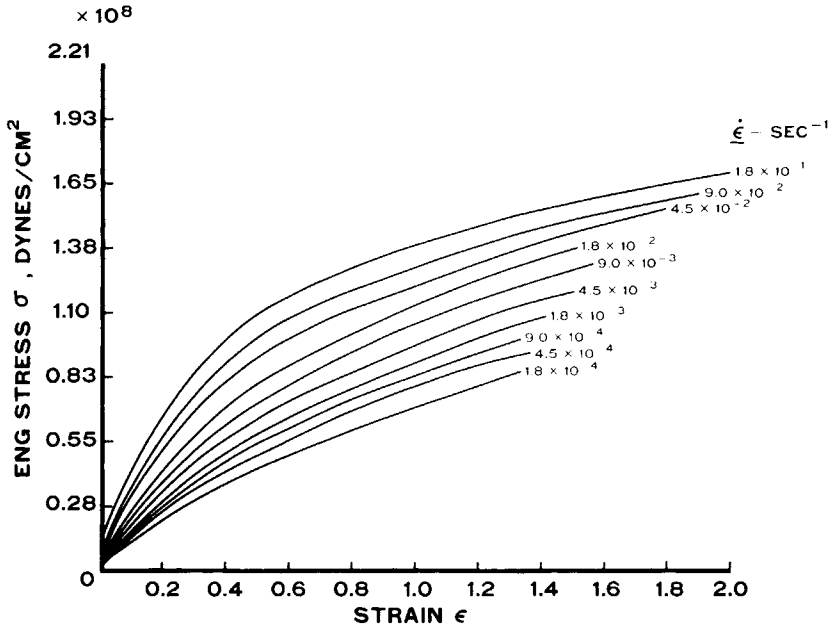


Fig. 2. Engineering stress/strain curves for various constant strain rates $\dot{\epsilon}$ at 23°C. Note terminal points on the curves indicate rupture.

## The Viscoelastic Function

Rupture characteristics will be related to time through viscoelastic properties.[14] In the Bueche-Halpin rupture theory, which will be used later in the analysis, it is desirable to have a viscoelastic function extending from the glassy to rubbery zones. This is necessary even though the rupture study spans only a part of the $\alpha$-transition region, because strain rate conditions at the tips of intrinsic or preformed cracks are such that macroscopic rupture properties may be shifted along the experimental time scale, usually toward shorter times.

A viscoelastic spectrum for Young's relaxation modulus is shown in Figure 3 for the plasticized PVC at a temperature of 23°C. Data points represent experimental values obtained by Tobolsky,[10] and the curve through the points is the arctan function,

$$\log_{10} E(t) = B_1 + B_2 \tan^{-1} [B_3(\log_{10} t - B_4)] \tag{2}$$

where $E$ is the relaxation modulus in dynes/cm$^2$, $t$ is the time in sec, and $B_1$, $B_2$, $B_3$, and $B_4$ are the constants 8.99212, −0.91406, 0.36242, and −1.28556, respectively. $B_1$ and $B_2$ are expressible in terms of the relaxed $E_r$ and unrelaxed $E_u$ moduli as follows:

$$B_1 = \frac{1}{2} \log_{10} E_u E_r, \qquad B_2 = \log_{10} \frac{E_r}{E_u}. \tag{3}$$

Tobolsky[10] gives limiting values for $E_r$ and $E_u$ as $4.0\times10^7$ and $2.5\times10^{10}$ dynes/cm$^2$, respectively. These same limiting values predicted from the arctan function eq. (2) are $3.6 \times 10^7$ and $2.68 \times 10^{10}$ dynes/cm$^2$, respectively.

Thus, the function appears to be a good representation of the experimental data.

Time to rupture $t_f$ in the present study will range from roughly 1 to 10,000 sec on the time scale of Figure 3. This is the part of the $\alpha$-transition region where $t_f \geq \tau$, the material relaxation time being $\tau$. Also this is where more than likely a nonlinear constitutive equation may be developed having separable time and strain effects on stress.

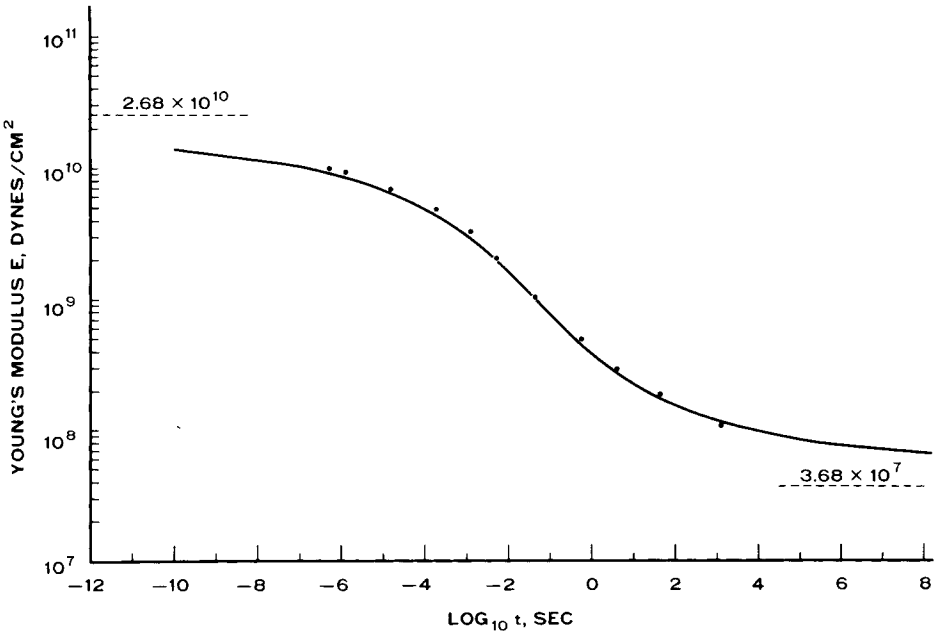


Fig. 3. Mechanical dispersion spectrum for Young's longitudinal relaxation modulus. Solid curve is eq. (2) and data points are from reference 10. Weight fraction of plasticizer in the PVC is 0.2958. Temperature is 23°C. Characteristic reference temperature is 12.97°C.

The arctan function eq. (2) was originally fitted to Tobolsky's[10] modulus data that were on a master curve having an extended time scale at 23°C and referenced to a characteristic temperature $T_i$ = 15°C. This characteristic temperature was found to be dependent on plasticization level as follows:

$$T_i = T_g - kw \tag{4}$$

where $T_g$ is the glass transition temperature for unplasticized PVC, 81°C; $k$ = 230, a constant; and $w$ is the weight fraction of plasticizer. Tobolsky's modulus data were for a weight fraction $w$ = 0.286; however, in the present study the plasticization level is at $w$ = 0.2958, which is based on the sum of the levels for the DOP and the M-275 thermal stabilizer. Consequently, it was necessary to translate or shift the arctan function along with the Tobolsky modulus data in order that they coincide with the temperature $T$ = 23°C and the characteristic temperature $T_i$ = 12.97°C of interest in the present inquiry. Actually, the shifting is a translation of the data along the time scale and is

made possible by a Williams, Landel, and Ferry[15] time–temperature equivalence equation modified by Tobolsky[10] as follows:

$$\log_{10} a = \log_{10} \frac{K(T)}{K(T_i)} = -\frac{16.4\ (T - T_i)}{56 + T - T_i} \tag{5}$$

where $K(T)$ and $K(T_i)$ are characteristic relaxation times at $T$ and at characteristic temperature $T_i$, respectively. Substituting $T = 23°C$ and $T_i = 12.97°C$ yields a value of $\log_{10} a = -2.45168$, which, then divided into $B_4$, produces the necessary shift in the arctan function eq. (2). Figure 3 is based on shifted data. It should be recalled that $B_4$ is the inflection point of the function along the time axis.

The glass transition temperature of the plasticized PVC is −18°C, which was obtained on a torsional pendulum device.[16]

## Constitutive Considerations

An analysis[3] of rupture in viscoelastic bodies such as polymers should not be treated as a separate phenomena but rather as part of the larger problem of describing their stress/strain time properties, or a constitutive equation. If these properties are considered as a three-dimensional surface, then rupture represents some limiting value or discontinuity on this surface or boundary to it.

Using the stress/strain curves in Figure 2, an attempt was made to derive a nonlinear constitutive equation by application of a graphic method developed by Smith[17] and Sips.[18] The key plot is the stress/strain isochrone, specifically $\log_{10}$ (true stress) against $\log_{10}$ (strain); $\log_{10} \lambda\sigma$ versus $\log_{10} \epsilon$ at constant time $t = \epsilon/\dot{\epsilon}$, where $\epsilon$ is the strain and $\dot{\epsilon}$ is the strain rate. Actually selection of $t$ is arbitrary, but for the present study failure time $t_f$ was selected. True stress $\lambda\sigma$ is the product of the extension ratio $\lambda$ and the engineering stress $\sigma$. It is the tensile stress acting on a cross section of the material in a deformed state, assuming negligible volume deformations, which is a reasonable assumption since no volume strains[20] greater than 5% were actually detected for longitudinal strains up to 140%. There were ten $\log_{10} \lambda\sigma$-versus-$\log_{10} \epsilon$ isochrones; one for each failure time $t_f$ from 11.9 to 7450 sec. They were approximately linear and displaced parallel to each other along the $\log_{10} \lambda\sigma$ axis. Each isochrone was normalized to a unit constant strain rate modulus $F(t_f)$, which is a shift factor in reducing isochrones to a master curve. The results in the form of a $\log_{10} \lambda\sigma/F(t_f)$-versus-$\log_{10} \epsilon$ plot are shown in Figure 4.

The ten stress/strain isochrones, each terminating in a rupture condition, are seen to scatter around a master isochrone whose slope is unity. A statistical analysis reveals that the composite slope based on all of the experimental isochrones is 1.026, with a multiple correlation coefficient of 0.9946. The implication is that, at least to a first approximation, the nonlinear constitutive stress/strain equation for the plasticized PVC under a uniaxial constant strain rate history is of the general form

$$\sigma = \Psi(t)\phi(\epsilon) \tag{6}$$

or in a more specific form

$$\lambda\sigma = F(t)\epsilon \tag{7}$$

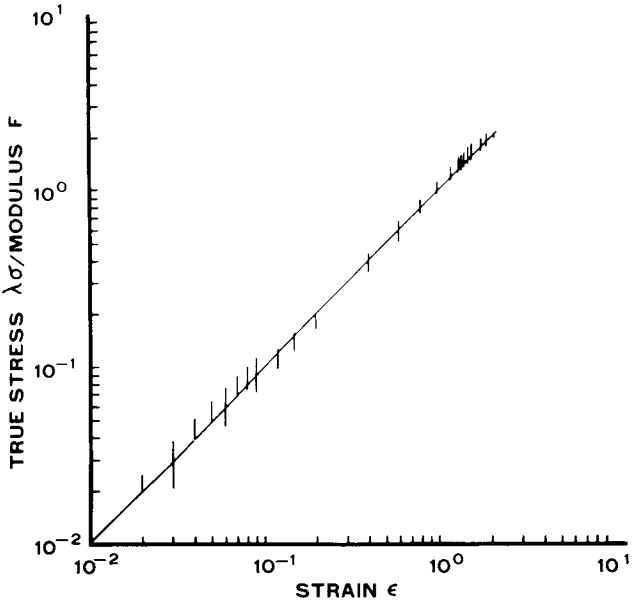


Fig. 4. Solid line is a master isochrone. Time $t$ for each isochrone is failure or rupture time $t_f$. Constant strain-rate modulus $F(t)$ is the shift factor for each isochrone along the true stress $\lambda\sigma$ axis. Scatter bands are limits of scatter for the ten isochrones.

where $\Psi(t) = F(t)$ and $\phi(\epsilon) = \epsilon$. Stress appears to be factorable into a product of two functions one of time and the other of strain, with the time function being equal to the constant strain rate modulus $F(t)$.

Equation (7) is an approximation to the nonlinear constitutive behavior primarily because it represents only a fair reproduction of the original stress/strain data in Figure 2; in some cases, the deference between experimental and predicted value is as high as 15%. One of the chief difficulties is determining the constant strain rate modulus $F(t)$ under sufficiently small deformations. If this is not a small deformation modulus, it is not readily relatable to Young's relaxation modulus, and it may not approach the Young's equilibrium modulus in the rubbery zone. This latter characteristic is important in determining whether or not eq. (7) is an equilibrium nonlinear constitutive equation.[1] Nevertheless, despite its approximate form, eq. (7) will be useful later on in the rupture analysis. In Table I, the constant strain-rate moduli, or normalization factors, are listed for each of the ten stress–strain isochrones composing the master isochrone in Figure 4.

According to Smith[19] et al., in a nonlinear constitutive equation such as eq (7), relaxation processes usually reflected in small deformation moduli should be accounted for in $F(t)$. If a finite strain perturbs such processes or activates additional ones, then the strain function $\phi(\epsilon)$ may exhibit time dependence. When time and strain effects are truly separable, rupture becomes the terminus of a nonlinear process in which time effects can be accounted for in small deformation moduli, the relaxation being invariant with respect to large deformations.

In recent attempts[20] to determine a more precise form for eq. (7), stress/strain isochrones from 1 to 300 sec were developed at small enough strain that

TABLE I
Normalization Factors For Stress/Strain Isochrones

| Failure time $t_f$, sec | Constant strain rate modulus $F(t_f)$,dynes/cm$^2$ | Failure time $t_f$, sec | Constant strain rate modulus $F(t_f)$, dynes/cm$^2$ |
|---|---|---|---|
| 11.9 | $2.68 \times 10^8$ | 335.1 | $1.80 \times 10^8$ |
| 21.4 | $2.27 \times 10^8$ | 787.2 | $1.67 \times 10^8$ |
| 39.9 | $2.31 \times 10^8$ | 1482.2 | $1.56 \times 10^8$ |
| 84.3 | $1.97 \times 10^8$ | 3051.1 | $1.52 \times 10^8$ |
| 175.0 | $1.87 \times 10^8$ | 7450.0 | $1.49 \times 10^8$ |

$F(t)$ was a small deformation modulus. Up to 10% strain, the average slope of the isochrones was 0.9914, and the maximum difference between the calculated and experimental strain values was only 1% at 10% strain, the calculated value being obtained from eq. (7). This implies that the plasticized PVC, at least on the lower end of the 10% strain range, is linearly viscoelastic, and additional evidence is given in the appendix where Young's relaxation modulus in Figure 3 is transformed into Young's dynamic storage modulus, the loss modulus, and the loss tangent. It is believed that the strain function in eq. (7) is not actually linear above 10% strain but is nonlinear due to temporal or strain effects, or a combination of both. This was very evident in the stress/time plots which are more or less intermediate plots in the Smith[17] procedure for developing stress/strain isochrones. These plots exhibited a strain dependence. Further evidence could be seen in results obtained from a Rheovibron[20] apparatus in which dynamic viscoelastic properties were evaluated at various large static extensions up to 116%, the lowest rupture strain $\epsilon_f$ being 133%. As the static strain increased, Young's storage modulus also increased, the loss modulus went through a shallow minimum, and the loss tangent decreased very noticeably. Consequently, it appears as though the deformation function $\phi$ in eq. (7) may contain the time variable; if not, it will be a nonlinear function of strain. Further developments on the strain function may be guided according to the work of Smith,[1] Haward,[22] and Halpin.[21]

Thus, eq. (7) will approximate the property surface in $\sigma$, $\epsilon$, $t$ space. It embodies two of the three functions needed to specify the rupture line. One is the time function $F(t)$; the other a deformation function $\phi(\epsilon)$. The third function can be either the true rupture stress $\lambda_f\sigma_f$ or rupture strain $\epsilon_f$ expressed as a function of rupture time $t_f$. Rupture data in Figure 2 will now be analyzed by projecting the rupture line onto the three coordinate planes, $\lambda_f\sigma_f$ versus $\epsilon_f$, $\lambda_f\sigma_f$ versus $t_f$, and $\epsilon_f$ versus $t_f$.

## Failure Envelope

In Figure 5, true rupture stress $\lambda_f\sigma_f$ is plotted against rupture strain $\epsilon_f$. This is a failure envelope, a projection of the rupture line onto the $\lambda_f\sigma_f$, $\epsilon_f$ coordinate plane. Data points on the envelope are the rupture or terminal points from all of the stress/strain curves, which were averaged to obtain Figure 2, or from all of the stress/strain isochrones shifted to obtain the composite isochrone of Figure 4. As one moves upward along the envelope, the

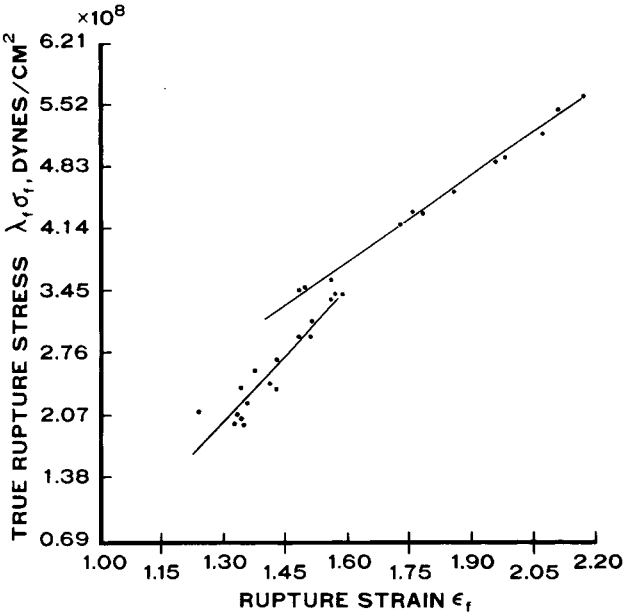


Fig. 5. Failure envelope. Transition in the envelope can be seen at a rupture strain $\epsilon_f = 1.52$. Corresponding failure times $t_f$ for the rupture stresses $\sigma_f$ and strains $\epsilon_f$ are given in Figs. 7 and 8 or Table I.

strain rate ranges from $1.8 \times 10^{-4}$ to $1.8 \times 10^{-1}$ $sec^{-1}$ or, in terms of rupture times $t_f$, from 7450 to 11.9 sec. In Figure 3, these times extend from the rubbery region into the transition zone.

It has been established[23] that rupture stress for amorphous elastomers is related to the ability of the material to dissipate mechanical energy. Some of the various dissipation mechanisms that have been identified are viscoelasticity,[23] crystallization,[2] molecular orientation,[25] network redistribution,[23] and cavitation.[1] Energy dissipation prevents the build-up of stored elastic energy at the tips of growing cracks or defects; thus, crack growth is suppressed. As long as crack growth is inhibited, rupture stress can be increased, in many cases in proportion to the dissipation. These are the concepts basic to an interpretation of the failure envelope because crack nucleation and growth are the precursors to rupture in the plasticized PVC.

The failure envelope in Figure 5 reveals an ultimate property transition at a failure strain $\epsilon_f$ of 1.52. This will be a logical dividing point in the interpretations which follow.

## Below Transition

Later it will be shown that the rupture data on the plasticized PVC are very well explained by the Bueche-Halpin theory which views rupture as the termination of a nonlinear process and which considers time effects through small-deformation viscoelastic properties. Consequently, one of the chief dissipation mechanisms, particularly below the transition in the envelope, is associated with the viscous aspects of viscoelasticity.

An interesting feature of the envelope, especially on the lower end, is the

relatively high degree of data scatter. This makes rupture appear as a fracture process having brittle characteristics in which the rupture stress itself is sensitive to some local material defect, probably a varying intrinsic subscritical crack size. The low viscous energy dissipation associated with the rubbery region will tend to couple together crack size with rupture stress, resulting in the latter showing a high degree of scatter. Notice, however, that as the strain rate increases upward along the envelope, data scatter diminishes very dramatically, and the rupture stress increases. Both are demonstrations of the effects of viscous energy dissipation at intrinsic crack tips. These comments on the envelope below the transition are in line with Harwood[23] who pointed out that the energy to propagate cracks in the rubbery regions of amorphous elastomers is only about two orders of magnitude higher than true surface energy.

Details will be given later of an optical microscope examination of a crack tip slowly propagating at a strain rate associated with the lower end of the envelope. The examination revealed the nature of the material-separation process involved in advancement of the crack tip. The material appears to exhibit a local microscopic yield phenomenon with rupture occuring immediately following the yield, in other words, between yield and what would be considered a drawing condition if the rupture had not occurred. This is a form of strain softening or plastic instability[25,22] during a yield drop. The actual material separation of the crack faces has all of the characteristics of ductility with the corresponding deformations being shear. Consequently, below the transition in the envelope the rupture process in the plasticized is tied into plastic instability.

## Above Transition

At the transition, a striking change occurs in the rupture process at the crack tip. Apparently, the strain rate has attained a critical value such that viscous dissipation has inhibited crack growth to a point where the material undergoes cold drawing. In place of the plastic instability developing during the microyield drop, as already pointed out, that occurs below the transition, there is a change to plastic stability at the transition and consequently the material goes into a cold draw mode of deformation. Thus, the upper part of the envelope is characterized in part by deformations associated with a drawn material. Here, crack growth is not only inhibited by viscous dissipation, but also by molecular orientation or, according to Haward,[22] orientation hardening.

Some evidence of the cold drawing is given in the $\epsilon_p$-versus-$\log_{10} t_f$ plot of Figure 6. Plastic strain $\epsilon_p$ is the residual strain based on the initial undeformed gauge length of a rupture specimen and the length remaining 30 days after the rupture test. It is seen that plastic strain decreases with rupture time $t_f$ until $t_f$ = 85 sec, which is the transition time on the envelope; then it increases very rapidly with further decreases in rupture time. This increase in plastic strain is expected on the basis of cold drawing.

Moreover, Haward[22] gives the characteristic necking strain for PVC as in the range from 0.4 to 1.5. This is a minimum strain requirement for orientation hardening. The upper limit of strain on Haward's 0.4-to-1.5 range is

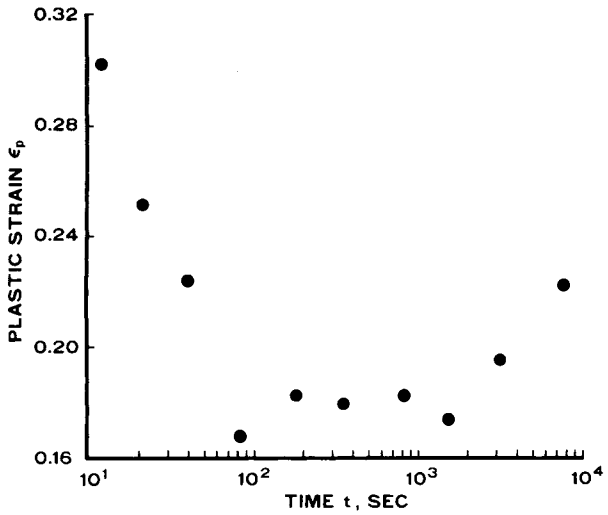


Fig. 6. Below $t_f$ = 84.3 sec the plastic strain component increases very rapidly with a decrease in rupture time.

close to the strain $\epsilon$ = 1.52, which is where the transition occurs on the envelope. In addition, the FPC 9282 PVC resin used in the plasticized PVC composition was dissolved in THF (tetrahydrofuran) and cast into a film from solution. Because the film was not allowed to dry completely, it stretched homogeneously when strained at a rate comparable to a strain rate on the upper part of the envelope. After the prestretched or cold-drawn film was dried, a preformed crack would not propagate perpendicular to the stretch direction. This is the crack behavior expected in a material that had undergone molecular orientation through cold drawing; thus, the conditions for cold drawing apparently exist on the upper part of the envelope.

Landel et al.[3] discuss statistical implications based on the way rupture data scatter around the failure envelope. It is noted that below the transition, data scatter changes markedly with strain rate and at the transition there is a sudden and a more dramatic change. On the upper part of the envelope data scatter not around, but along the envelope as the strain rate increases. This implies that the statistical distribution for the rupture properties, that is, $\lambda_f\sigma_f$ and $\epsilon_f$, are nearly identical. If one is skewed, so is the other, the chief difference being a change in scale. However, nothing is known about the underlying statistical distribution which could be specified in terms of crack characteristics, such as size.[11] The radical change in data scatter at the transition signifies an equally abrupt change in the dependencies in rupture behavior. Below that point, as already pointed out, rupture depends on some local defect property, probably an intrinsic subcritical crack size; and above the transition, the dependency may change to a bulk material property, probably the work to rupture. No matter what the change, the balance between stored elastic and dissipation energies at the crack tip favors higher rupture values.

The failure envelope is a profile of rupture behavior through the $\alpha$-transition zone. Starting with the rubbery response on the lower end of the envelope, an increase in strain rate moves the rupture characteristic, that is, $\lambda_f\sigma_f$

and $\epsilon_f$, upward along the envelope terminating in a true rupture stress of 5.38 $\times 10^8$ dynes/cm$^2$, the highest obtainable in the present inquiry. The corresponding rupture time $t_f$ is 11.9 sec, which is about a decade higher than the material relaxation time in the center of the $\alpha$-transition as seen in Figure 3. From the trends indicated on the upper part of the envelope, rupture stress may continue to increase with strain rate, reaching into the glassy zone. This, however, will be contingent on inhibiting subcritical crack growth through elastic energy dissipation, and probably a more cogent factor would be an adiabatic temperature condition usually associated with a high strain rate. The failure envelope[1] for a crosslinked amorphous elastomer normally proceeds in an upward direction where the material reaches a limiting extension, then turns in a counterclockwise direction, finally tracing out a path parallel to the rupture strain axis that would be indicative of a glassy response. It is interesting to note that the range of maximum true rupture stresses[26] for a wide variety of highly crosslinked elastomers is from $5.52\times10^8$ to $11.03\times10^8$ dynes/cm$^2$. A glassy value[20] for an unplasticized rigid PVC is $5.83\times10^8$ dynes/cm$^2$, with a corresponding failure strain of slightly less than 5%. These values make an interesting comparison with the maximum of $5.38\times10^8$ dynes/cm$^2$ attained on the plasticized PVC.

An average rupture value for the three rupture tests at each strain rate on the failure envelope can be predicted within about 4% using the Bueche-Halpin rupture theory along with a curve-fitting procedure to be discussed in the next section. This is the degree to which the failure envelope is predictable from a rupture model.

## Dependence of $\lambda_f\sigma_f$ on Rupture Time $t_f$

In Figure 7, experimental true rupture stress $\lambda_f\sigma_f$ is plotted against $\log_{10} t_f$. Each data point is the mean of three tests. Relations between these two variables in the $\lambda_f\sigma_f$, $t_f$ coordinate plane may be selected as one of the three independent equations necessary to describe the rupture line in three dimensions, the other two being $F(t)$ and $\phi(\epsilon)$.

Figure 7 will be analyzed in the light of the Bueche-Halpin rupture theory that is based on the interplay between the fracture and stored elastic energies and on the assumption that rupture involves crack nucleation, subcritical growth, and catastrophic propagation; time for the first two phases is equivalent to rupture time $t_f$. Time for catastrophic propagation is usually so small as to be neglected. The Bueche-Halpin theory has never been appraised for relative merits and deficiencies, nevertheless, it is conceptually correct and should provide a basis for analysis and subsequent development.[1]

An assumption underlying the theory is that rupture is the terminus of a nonlinear process in which time effects are assessable from small-deformation viscoelastic properties evaluated at $t = t_f$. Consequently, the true rupture stresses in Figure 7 will be related to rupture time $t_f$ through Young's relaxation modulus as follows:

$$\lambda_f\sigma_f = KE\left(\frac{t_f}{q}\right). \tag{8}$$

Here, Young's relaxation modulus $E(t_f/q)$ is given by the arctan function eq.

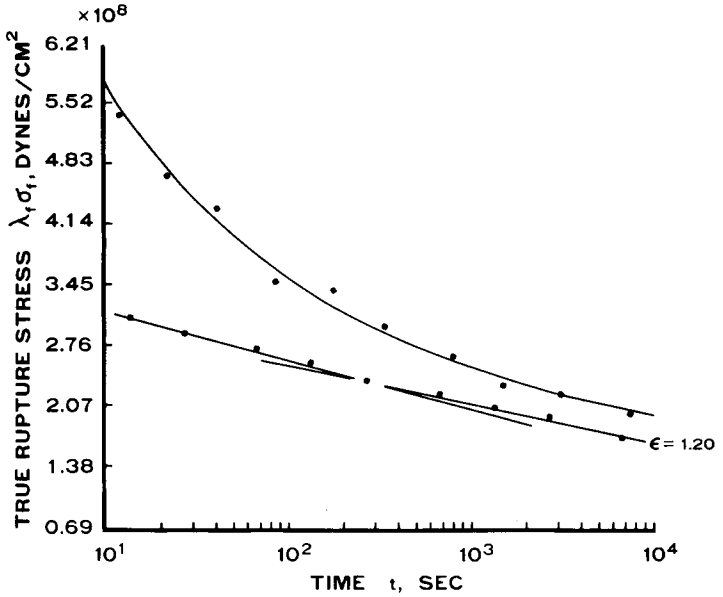


Fig. 7. Upper part of graph shows experimental data points for true rupture stresses, and the curve through the points is eq. (8). A distinct break can be seen in the true stress-versus-$\log_{10}$ time plot for a strain $\epsilon = 1.20$.

(2). $K$ is a constant which depends on a stress–concentration factor in the crack tip and also on a critical stress or strain condition existing in a material filament in the crack tip, prior to filament rupture. The constant $q$ represents the number of material filaments ruptured at the crack tip during subcritical crack growths. Actually, it is a shift factor along the time scale based on the difference between the time associated with the macroscopic rupture property and the time for microscopic rupture in the crack tip. This is considered in the arctan function eq. (2) by adding log $q$ to the constant $B_4$, thereby shifting the viscoelastic function along the time axis into coincidence with the rupture data.

To fit the experimental data in Figure 7 to eq. (8), the optimum values for $K$ and log $q$ turned out to be 1.762 and 0.6740, respectively. A new value for $B_4$ is −0.61154161. Some literature[1] values for $K$ are: $K = 1.0$ for an ethylene–propylene (EPR) vulcanizate and $K = 3.5$ for styrene–butadiene vulcanizates containing various amounts of carbon black filler. The corresponding $q$ value for the EPR material is $q = 10^4$. Equation (8) predicts the experimental rupture stresses in Figure 7 within 3.9%. Thus, viscoelasticity is a strong factor in the rupture process.

Actually, the viscoelastic function that should be used in eq. (8) is $F(t)$ and not $E(t)$, simply because the rupture tests were performed under a constant strain-rate history, which is the history used in evaluating the constant strain-rate modulus $F(t)$.[17] However, the viscoelastic spectrum for $F(t)$ from the glassy to rubbery regions is not known. The use of Young's relaxation modulus $E(t)$ in eq. (8) is tantamount to the assumption that rupture properties are not affected by strain history, a point requiring experimental verification.

On the strength of the precision with which eq. (8) explains the experimental data in Figure 7, energy dissipation at intrinsic crack tips is largely viscous. The transition, already pointed out on the failure envelope, is also evident in Figure 7 at rupture time $t_f$ = 85.0 sec. It is interesting to speculate on the deformation mechanisms in this rupture property transition.

Bauwens et al.[27,28] made a study of the relationship between intrinsic yield stress[6] and strain rate on rigid PVC. Temperatures ranged from −50° to 70°C and the strain rate ranged from $10^{-5}$ to $10^{-1}$ $sec^{-1}$; the strain rate was controlled on an Instron tensile machine. Plots of yield stress per unit temperature versus log strain rate, that is, $\sigma_y/T$ versus $\log_{10} \dot{\epsilon}$, were linear. In fact, over the range of available strain rates, two linear curves were required to represent the data; both were derived from the Ree-Eyring theory of non-Newtonian viscosity. These two linear functions, having different slopes, intersected, and Bauwens referred to the intersection as a secondary transition. At strain rates below the transition, the deformation processes were called alpha ($\alpha$), and above the transition they were called beta ($\beta$), the alpha and beta descriptions being arrived at from an activation energy analysis. At 23°C, Bauwens data show the transition to occur at a strain rate of $5.3\times10^{-3}$ $sec^{-1}$. The slope or stress coefficient for the beta curve was $2.9\times10^7$ dynes/$cm^2$ and for the alpha curve, it was $2.0\times10^7$ dynes/$cm^2$. A stress coefficient from the Eyring rate theory is $kT/v$, where $k$ is the Boltzmann constant, $T$ is the temperature, and $v$ is an activation volume. Consequently, below the glass temperature the intrinsic yield stress/strain rate behavior of rigid PVC exhibits a transition that apparently reflects a change in the molecular deformation processes.

This transition in yield behavior and the behavior of the true rupture stresses (Fig. 7) for the plasticized PVC are so similar that it is tempting to conclude that the same deformation processes are operative in both, despite the fact that the glass transition temperature $Tg$ = −18°C for the plasticized PVC is far below the test temperature, 23°C.

In Figure 7, true rupture stress reveals an abrupt change at $t_f$ = 85.0 sec or a strain rate of $1.8 \times 10^{-2}$ $sec^{-1}$. This, of course, also identifies the transition already described on the failure envelope. At rupture time $t_f$ = 85.0 sec and below, the rupture stresses show a radical change in $\log_{10} t_f$ dependence as compared to the dependence at times greater than $t_f$ = 85.0 sec. A slope or stress coefficient analysis was made of the true stress $\lambda\sigma$ versus $\log_{10} t$ curves which terminated in the true rupture stresses shown in Figure 7. The curves were linear to rupture with stress coefficients ranging from $2.16 \times 10^7$ up to $2.63 \times 10^7$ dynes/$cm^2$, and they increased in proportion to the rupture stress. Interestingly, these lie in the range between the stress coefficient values for the alpha and beta deformation mechanisms mentioned above in Bauwens analysis on rigid PVC. It is speculated that for times $t_f$ = 85.0 sec and greater in Figure 7, rupture behavior is dominated by the alpha process, and for times less than 85.0 sec the alpha process is augmented by the beta process, with the transition occuring at $t_f$ = 85.0 sec. This, also, would be fundamental to the transition in the failure envelope in Figure 5 and the plastic-strain behavior in Figure 6.

A true stress $\lambda\sigma$-versus-log $t$ curve for a strain $\epsilon$ = 1.20 is given in Figure 7 just below the rupture data. Note the stress/strain time conditions here are

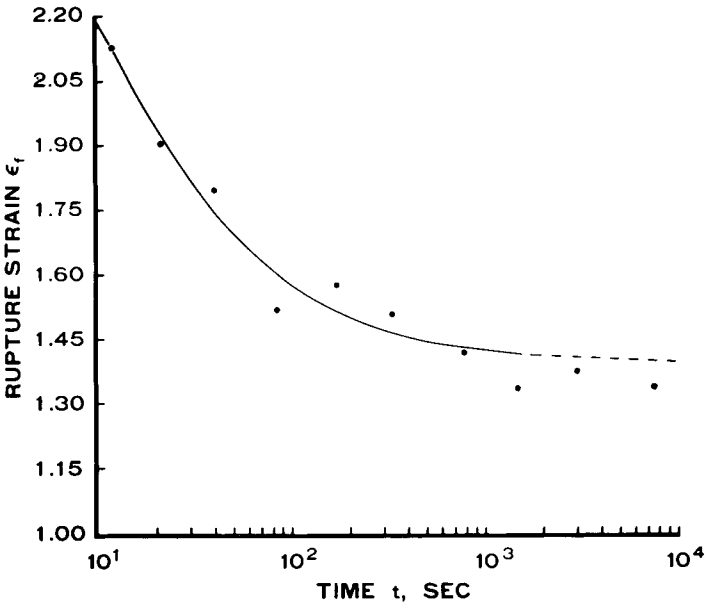


Fig. 8. Curve is obtained from eq. (9). At about $10^2$ sec, the transition effects in the rupture strain are more pronounced than they are in the rupture stress.

below those for rupture. If one examines these data closely, there are actually two linear $\lambda\sigma$-versus-log $t$ curves intersecting along the time axis at a time slightly greater than $t = 85.0$ sec. Stress coefficients for the two intersecting curves are $2.0 \times 10^7$ and $2.3 \times 10^7$ dynes/cm$^2$. This intersection, which apparently is greatly amplified in the rupture behavior, can be seen in all of the plots of $\lambda\sigma$ versus log $t$ for strains down to 20%.

## Dependence of $\epsilon_f$ on Rupture Time $t_f$

The profile of the rupture line in the $\epsilon_f$, $t_f$ coordinate plane is given in Figure 8. According to the Bueche-Halpin rupture theory, rupture strain in this coordinate plane can be predicted from

$$\epsilon_f = \frac{KE(t_f/q)}{F(t_f)}. \tag{9}$$

This is the nonlinear constitutive relation eq. (7) with eq. (8) substituted for the true stress and a time function $F(t_f)$ substituted for the constant-strain rate moduli, listed in Table I. Both eqs. (8) and (9) were fitted to the rupture data using a computer program in which the equations were considered simultaneously and the constants optimized were not only $K$ and $q$, but also the constants in the empirical time function for $F(t_f)$. This procedure has a potential for developing internal consistency among the functions representing rupture data in the three coordinate planes. Equation (9) fits the rupture data in Figure 8 within a mean error of 3.9%. The equation was not extended beyond time $t = 2000$ sec because of a slight instability in the function for $F(t_f)$.

In Figure 8, one can again see the transition effects at $t_f = 85.0$ sec, which

were already discussed for the other two coordinate planes. Apparently, there is a large component of anelastic strain in the rupture strains of Figure 8. This can be seen by noting the difference between the rupture strain in Figure 8 and the plastic strain for the corresponding time in Figure 6. The difference is the anelastic strain component.

Equation (9) indicates that extension is strongly dependent on viscoelasticity over the narrow range of rupture time involved. Consequently, extension may be controlled by viscous energy dissipation which Eirich et al.[2] point out is true for a great many amorphous polymers. Therefore, there is a possibility that extension will maximize on the time axis with viscous energy dissipation. This brings into the picture dynamic viscoelastic properties, namely, the dynamic Young's storage modulus, the loss modulus, and the loss tangent. These are given in the appendix for the plasticized PVC for use in future analyses in which the rupture characteristics are determined over a more extensive range on the time scale, preferably from the glassy to the rubbery region. Landel[3] discusses interesting correlations between the dynamic viscoelastic functions and rupture properties.

## Optical and Electron Microscopy

In all rupture tests, the plasticized PVC deformed homogeneously to rupture and exhibited stress whitening. The latter was barely visible at low loads but increased in intensity very rapidly just prior to rupture. It was most intense and exceptionally noticeable where a crack nucleated and developed its subcritical growth. Consequently, based on visual observations of the ring specimens under uniaxial extension, rupture was preceded by the nucleation, subcritical growth, and catastrophic propagation of cracks.

More detailed evidence on these three regimes of crack growth is shown on the scanning electron micrograph of Figure 9. This is a view of a rupture surface on a test specimen that had bgen exposed to a strain rate on the lower part of the failure envelope. The white ridges and dimples were formed by the ductile or distortional deformations at the crack tip and are characteristic surface markings of a subcritical growth stage. This is the morphology that covered most of the rupture surface at the lower end of the range of strain rates.

However, as the strain rate increased upward along the envelope, the subcritical crack growth area decreased accordingly as can be seen by comparing the SEM micrographs in Figures 9 and 10. The latter shows the surface of a specimen that had been exposed to the highest strain rate. Here, the subcritical crack growth area covers only a small part of the rupture surface, and the boundary between this area and where the crack began its high-velocity propagation is very evident. Apparently, the transition in the failure envelope also reflects some form of transition in subcritical crack morphology, as will be pointed out in more detail later. The micrographs in Figures 9 and 10 indicate that rupture in the plasticized PVC is a heterogeneous process involving crack nucleation and growth.

The nucleation phase is not understood. Initiation of the crack seems to occur on the specimen surface, thus there is a possible relationship between the stress whitening and nucleation. The two may be more readily linked if

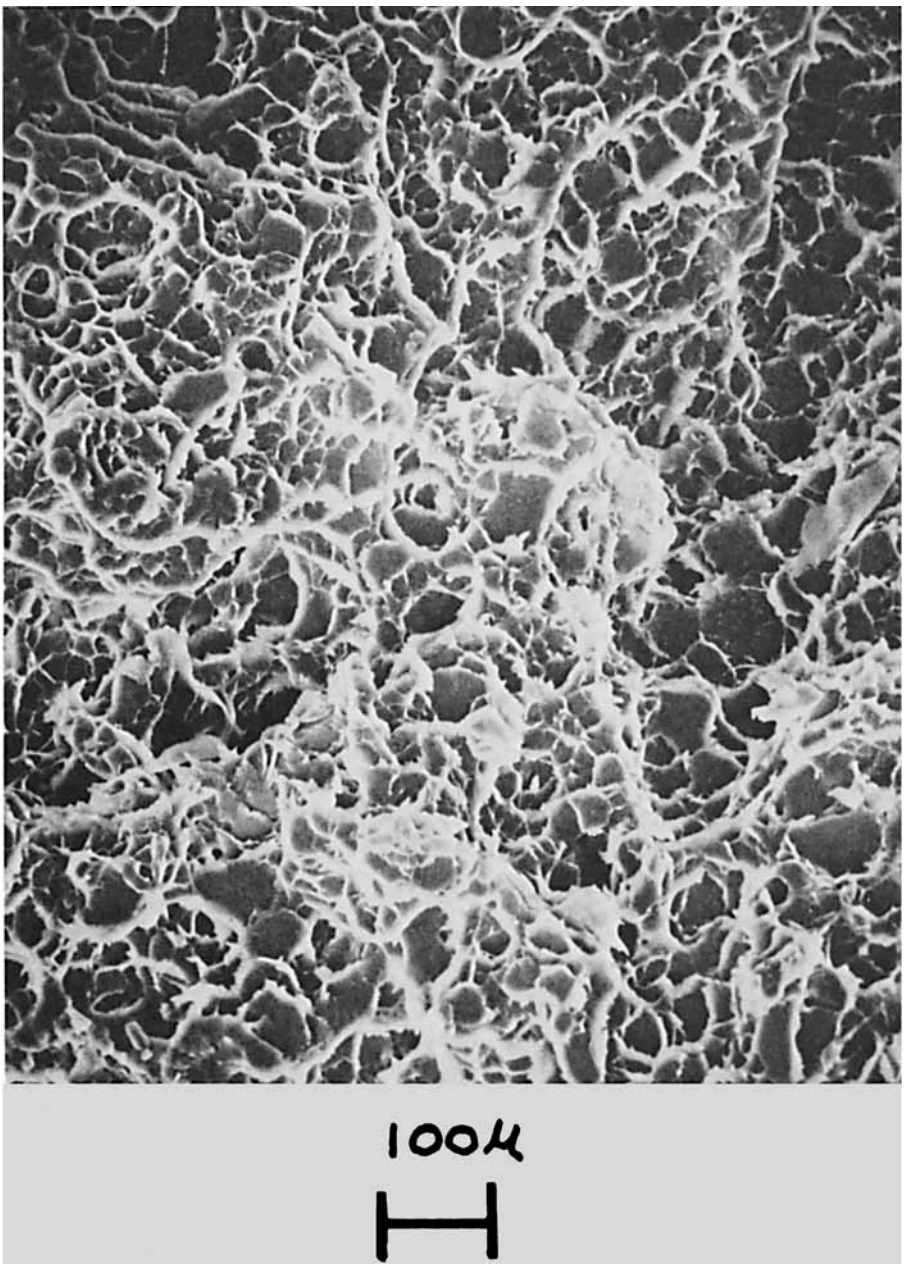


Fig. 9. SEM micrograph showing cavitation effects on the rupture surface for very low strain rates. This is the subcritical crack growth morphology.

the former could be identified as stress crazing that is the precursor to fracture in amorphous polymers.[6,5] One of the interesting implications of eq. (8) is that nucleation is either independent of time or has the same time dependence as the rupture stress. There is evidence that the surface of plasticized PVC under tension develops step-like features when the stress approaches rupture levels. They may be seen at about 500× magnification in reflected

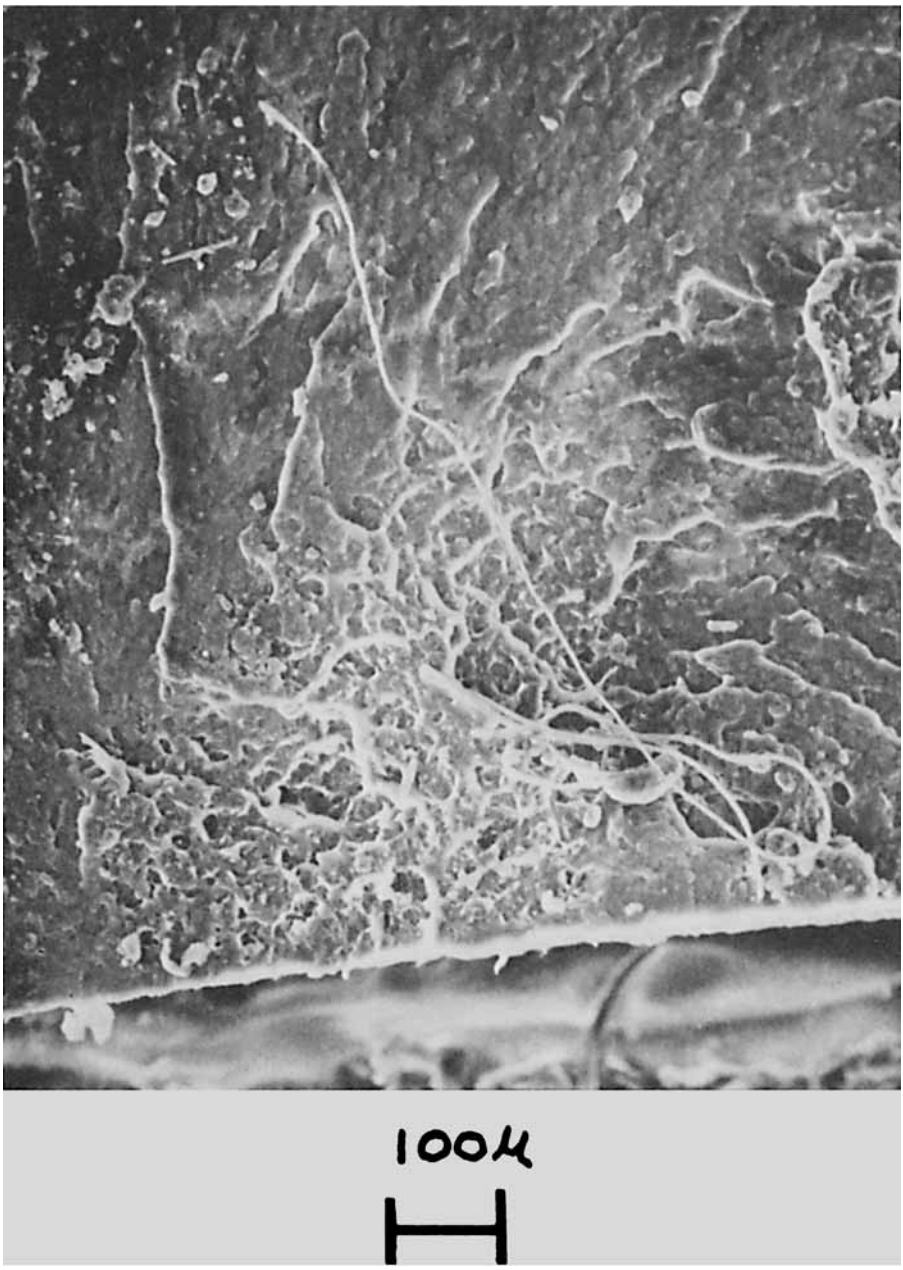


Fig. 10. Subcritical crack morphology at the highest strain rate. Note the morphology covers only a small portion of the total rupture surface.

light under a Leitz research microscope. Conceivably, the steps may be the protrusions of microshear bands as discussed by Yeh.[20]

The subcritical crack growth area in Figure 9 reveals strong indications of cavitation in the material. This is indicated by the crater-like depressions outlined or bounded by highly extended material, that is, the ductile dimples and ridges showing up as white on the micrograph. There are two lines of ev-


Fig. 11. Same as Fig. 9 with the dimples and ridges magnified to illustrate ductile deformations associated with ruptured filaments at the crack tip.

idence that indicate that cavitation develops in the stress field just ahead of a crack tip rather than developing throughout the volume of the material when it is exposed to loads. First, no volume strains greater than 5% have been detected for homogeneous extensions up to 140%. The second evidence and the source of the most precise data to date has been obtained from observations on the dynamics of crack-tip behavior as viewed under a Leitz research microscope.

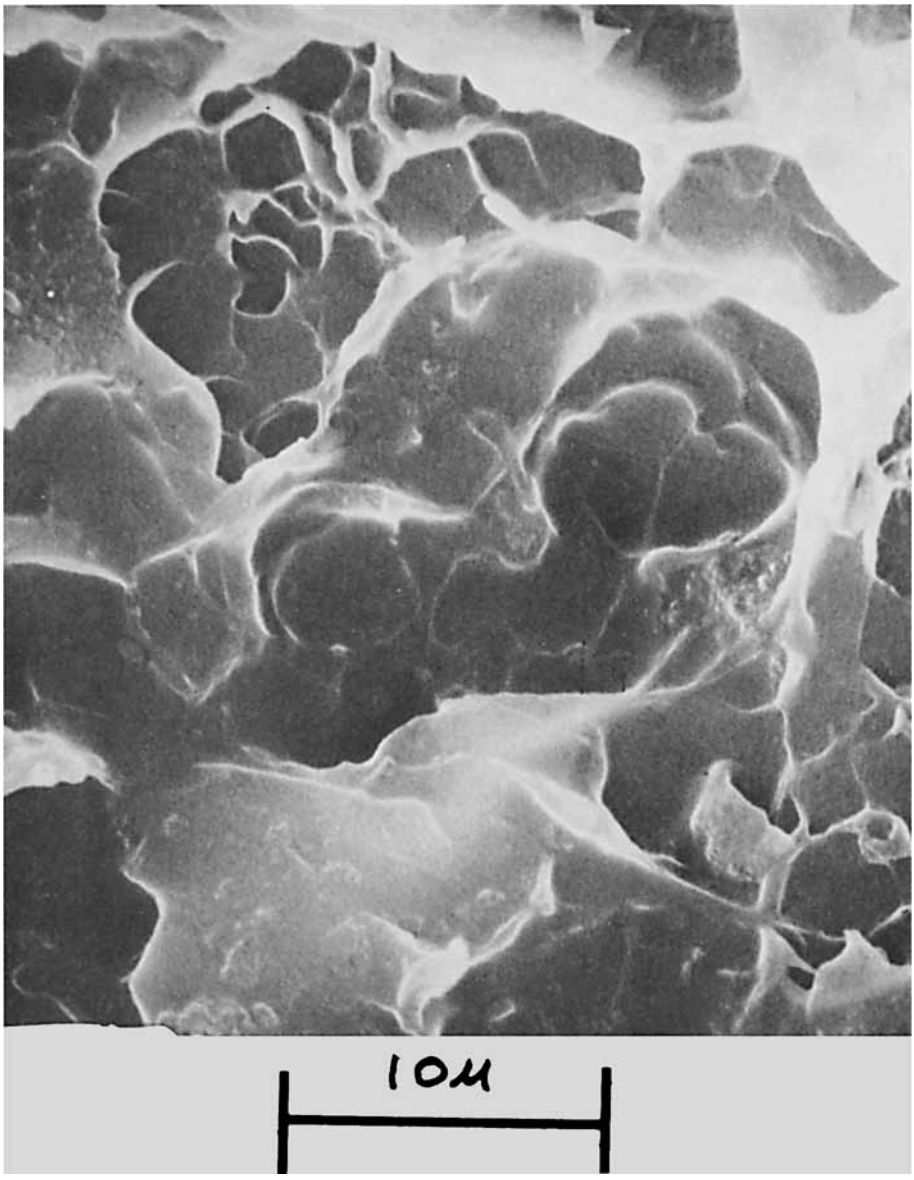


Fig. 12. Same as Fig. 10. This micrograph shows the change in the deformation associated with filament rupture at high strain rates.

Miniature tensile specimens 0.80×5.08 cm were fabricated from a film 0.05 cm thick. They were precracked, then installed and loaded in a microtensile tester at room temperature. The crack tip was viewed in both transmitted and reflected light under the Leitz research microscope at magnifications of 176× and 500×.

Microvoids were seen to nucleate a short distance ahead of a blunt crack tip. In the early stages of their growth, it was not possible to ascertain whether they were penny shaped or spherical. They enlarged under the influence of the stress field, and eventually, through the process of coalescence,

the walls between adjacent voids became very thin and broke up into filaments or ligaments. Interestingly, such a filament pattern is almost identical with that described in a variety of crack models; for example, the Bueche-Halpin[21] model for elastomers, the Kraft[30] plastic instability model for high strength steel, and the Williams et al.[31] plastic instability model for rigid PVC. Eventually, the filaments extend, neck down to diameters of microdimensions, and ultimately rupture in a completely ductile manner with the deformations at separation being primarily shear or distortional. These are the sequence of events that produced the cavitation effects and the pointed ends of ruptured filaments shown in the micrograph of Figure 9, a close-up view being shown in Figure 11. The sharp or pointed filament ends are manifestations not only of the sharp deformations associated with filament rupture, but also that crack growth proceeds isothermally rather than adiabatically.

The filament rupture just described is a description of the material separation process associated with subcritical crack growth at low strain rates, therefore, it is fundamental to the rupture process below the transition in the failure envelope. Probably the most meaningful description of filament rupture at the crack tip might be developed around the nomenclature used by Haward et al.[22,25] in pointing out certain characteristic features on the true stress/strain curve for thermoplastic polymers. First, a filament appears to exhibit a yield behavior; after this, with further extension, it develops a yield drop during which rupture occurs. In other words, the actual material separation takes place between yield and what would normally be a draw condition if there had been no separation. This is a form of strain softening or plastic instability. It is the final phase of separation for microvoid nucleation, growth, and coalescence at a subcritical crack tip, but only below the transition in the failure envelope.

Above that transition the dynamics of crack-tip behavior could not be observed directly; however, the changes that occur in filament rupture can be hypothesized from an analysis of the micrographs covering the rupture surfaces for each of the ten strain rates over the entire envelope.

The envelope transition can be characterized by the area of subcritical crack growth. Below that point this area covers almost all of the rupture surface as can be seen in Figure 9, and at the transition the coverage is reduced to about one half. Above the transition and at the highest strain rate, the subcritical crack area is reduced to a small fraction of the total-rupture surface morphology as shown in Figure 10. Also, the vertical depth of subcritical crack development is reduced. This is seen by comparing micrographs in Figures 9 and 10 and in Figures 11 and 12.

The micrograph in Figure 12 reveals a dramatic change in filament rupture which apparently occurs at the transition in the envelope and is applicable to the separation processes above that point. Instead of a filament rupturing because of strain softening or plastic instability, a plastic stability sets in which permits the filament to develop a cold draw mode of deformation. It does not rupture, but tears or cracks. This can be seen in the micrograph of Figure 12. Apparently, such a change in the material separation process not only is involved at the transition in the failure envelope, but also in the rupture characteristics in all three coordinate planes. Also involved would be the relaxation mechanisms which have already been discussed.

The formation of microvoids, which were pointed out as preceding the subcritical crack tip, may be the final phase of intrinsic crack nucleation. Such an interesting relation has not been established. Cavitation is not unique only to PVC or to amorphous polymers in general, but appears to be a characteristic of a wide variety of material as discussed by Kambour.[6] It could be that beyond the subcritical crack growth area shown in Figure 12, where the crack tip has attained catastrophic velocity, the separation mechanisms might be those involved in the cavitation. At such velocity, the crack tip is sharp, and material separation occurs in a small volume around the tip resulting in a very smooth rupture surface morphology.

## SUMMARY

Rupture characteristics for a plasticized PVC on each coordinate plane, that is, the failure envelope, the rupture stress-versus-time function, and the rupture strain-versus-time function, all reveal a time dependence expected in the glass-to-rubber transition. However, another form of transition is also indicated in the ultimate properties. It is characterized by the onset of cold drawing, by abrupt changes in rupture characteristics, by changes in resistance to crack growth, and by changes in the statistical distribution for rupture data.

Experimental rupture data on the coordinate planes can be described by the Bueche-Halpin theory with time effects being accounted for by Young's longitudinal relaxation modulus, indicating that time and rate effects are associated with viscoelastic-constitutive behavior.

The rupture process is intrinsic crack growth which consists of microvoid nucleation, growth, and coalescence. Nucleation mechanisms are not defined; they may be related to stress crazing. Subcritical crack growth area and morphology on the rupture surface can be qualitatively related to the rupture characteristic. Both areas and morphology undergo changes through the ultimate property transition; in particular, the material separation deformations reveal a change from plastic instability to plastic stability, the latter being associated with cold drawing. There is evidence that the transition may be attributable to a nonlinear stress/strain effect on the secondary beta mechanism in PVC.

## Appendix

### Viscoelastic Functions

In this appendix, eq. (2), the viscoelastic function for Young's longitudinal relaxation modulus, will be employed to derive three other linear viscoelastic functions for plasticized PVC. They were derived as a test for linear viscoelastic properties in connection with the nonlinear constitutive, eq. (7), and for purposes of correlation[3] with the rupture strain-versus-rupture time function. However, the latter function must be known over a considerable range of experimental times in order to carry out the correlation.[3]

Within the framework of linear viscoelasticity, when one viscoelastic function is given, all others may be obtained from it. This is accomplished through a transform developed by Ferry and Williams[33] as follows:

$$H(\tau) = -M(m)E(t)\left.\frac{d\log_{10}E(t)}{d\log_{10}t}\right|_{t=\tau} \tag{10}$$

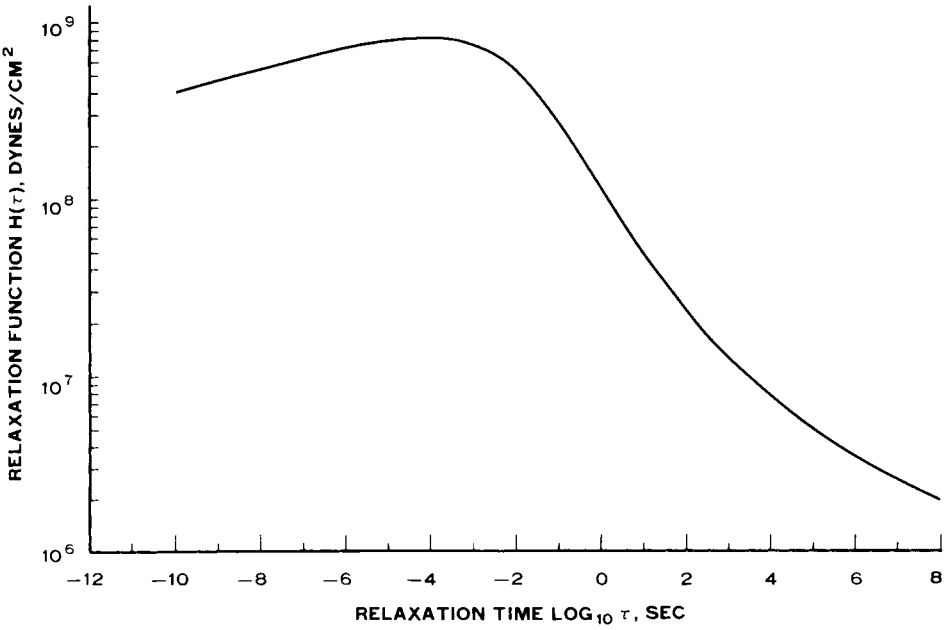


Fig. 13. Relaxation function derived from the mechanical dispersion spectrum for Young's longitudinal relaxation modulus. Solid curve is eq. (10).

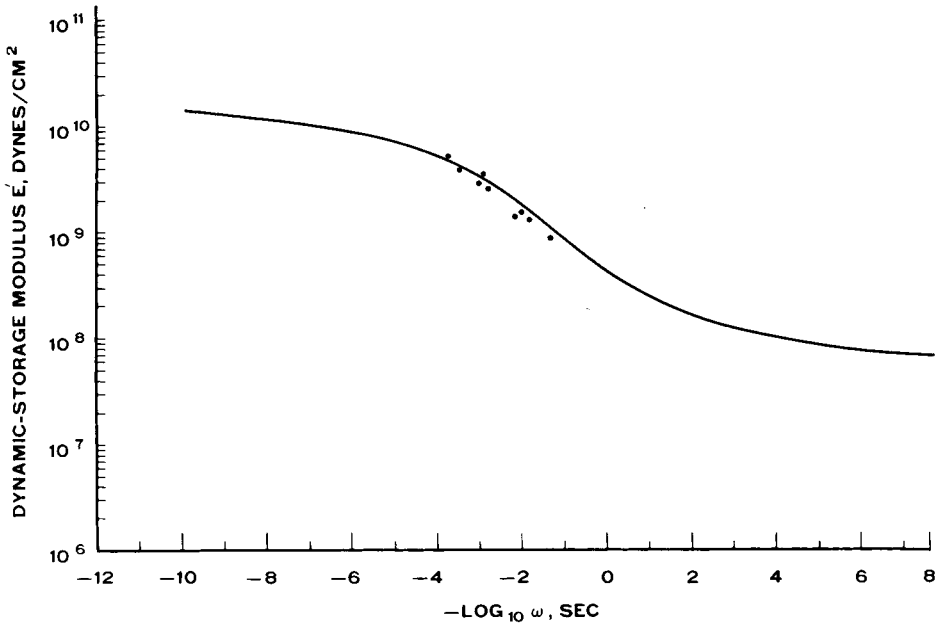


Fig. 14. Dynamic storage modulus $E'$. Solid curve is eq. (12). Black dots are experimental data obtained on the Rheovibron and a cantilever-beam instrument.

where $H(\tau)$ is the relaxation-distribution function, $\tau$ is a material relaxation time, $E(t)$ is Young's longitudinal relaxation modulus, and $M(m) = 1/\Gamma(1 + m)$. $\Gamma(1 + m)$ is the gamma function and $m$ is given by

$$m = -\frac{d}{d \log_{10} t} \log\left(-\frac{dE(t)}{d \log_{10} t}\right). \tag{11}$$

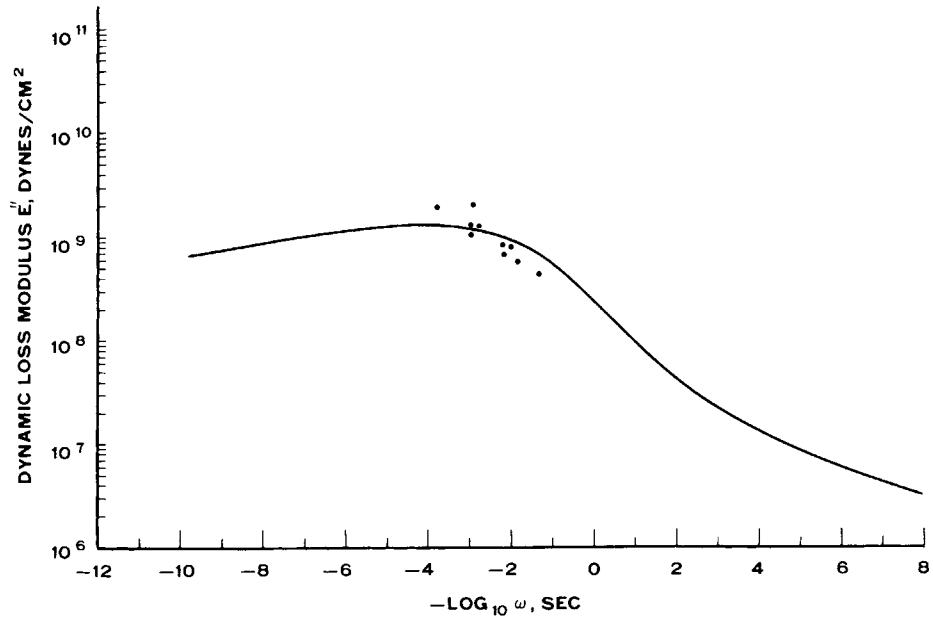


Fig. 15. Dynamic loss modulus $E''$. Solid curve is eq. (13).

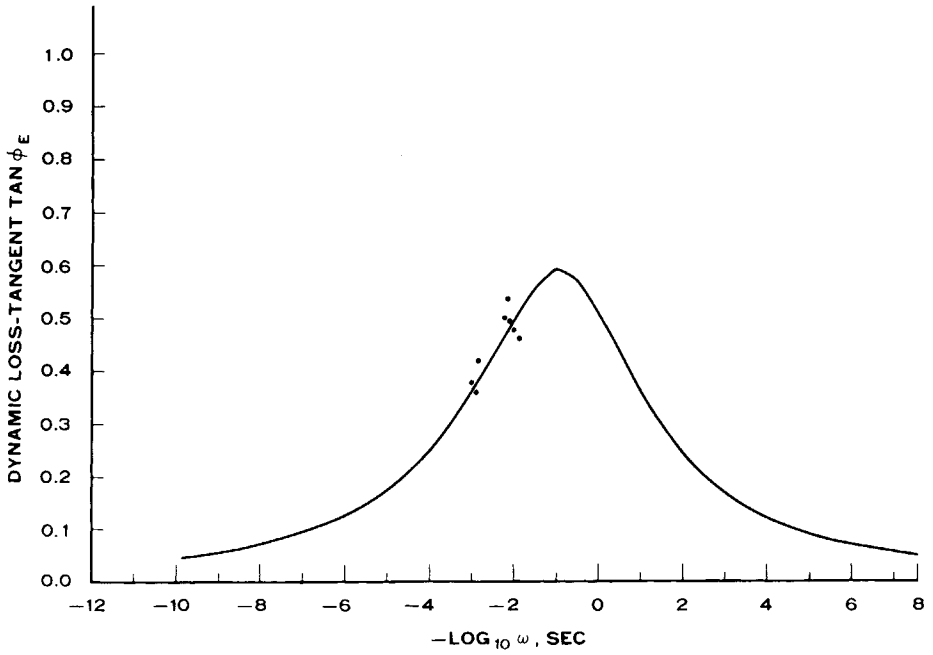


Fig. 16. Dynamic loss tangent tan $\phi_E$, eq. (14).

The arctan function, eq. (2), is substituted wherever $E(t)$ is indicated. The viscoelastic relaxation function $H(\tau)$ is given in Figure 13. It maximizes at $10^{-4}$ sec, which is far below the experimental times available on the Instron. The rubbery zone is not too sharply defined. Figure 13 agrees very favorably with the relaxation function $H(\tau)$ obtained from another transform developed by Schwarzl and Staverman.[33] Sommers in McCrum et al.[32] has determined the relaxation

spectrum for rigid PVC, and it makes an interesting comparison with the spectrum in Figure 13 for the plasticized PVC.

With the relaxation function $H(\tau)$ from eq. (10), it is now possible to calculate the dynamic viscoelastic properties, specifically, the dynamic longitudinal-storage modulus $E'$, the dynamic loss modulus $E''$, and the loss tangent tan $\phi_E$. These are obtained from the following equations[33]:

$$E'(\omega)_{\omega=1/t} = E(t) + H(\tau)\left[\frac{\pi}{2}\csc\frac{m\pi}{2} - \Gamma(m)\right]_{\tau=t} \qquad -1 < m < 2 \tag{12}$$

$$E''(\omega)_{\omega=1/t} = H(\tau)\left[\frac{\pi}{2}\sec\frac{m\pi}{2}\right]_{\tau=t} \qquad -1 < m < 1 \tag{13}$$

$$\tan\phi_E = \frac{E''(\omega)}{E'(\omega)}. \tag{14}$$

Equations (12), (13), and (14) are given in Figures 14, 15, 16, respectively. The experimental data points obtained from Rheovibron and cantilever beam instruments show that the transforms are reasonably correct; however, additional data are needed over a much larger time scale. Actually, with the relaxation spectrum $H(\tau)$, it is possible to calculate any of the other viscoelastic functions, for instance, the dynamic longitudinal storage compliance, the dynamic longitudinal loss compliance, and the retardation spectrum.

The author wishes to thank David C. Messersmith and Charles D. Nauman for the computer programming; Charles I. Sanders, James R. Rittenhouse, and Karl A. Gollatz for assistance in microscopy; and the Armstrong Cork Company for permission to publish.

## References

1. T. L. Smith, in *Rheology,* Vol. 5, F. R. Eirich, Ed., Academic Press, New York, 1969, p. 127.
2. F. R. Eirich, and T. L. Smith, in *Fracture An Advanced Treatise,* Vol. VII, H. Liebowitz, Ed., Academic Press, New York, 1972, p. 508.
3. R. F. Landel and R. F. Fedors, in *Fracture Processes In Polymeric Solids,* B. Rosen, Ed., Interscience, New York, 1964, Chap. IIIB, p. 361.
4. J. P. Berry, in *Fracture An Advanced Treatise,* Vol. VII, H. Liebowitz, Ed., Academic Press, New York, 1972, Chap. 2, p. 37.
5. S. Rabinowitz and P. Beardmore, *Crit. Rev. Macromol. Sci.,* **I,** 1 (1972).
6. R. P. Kambour, *J. Polym. Sci., Macromol. Rev.,* **7,** 1 (1973).
7. P. Beahan, M. Bevis, and D. Hull, *Polymer,* **14,** 96 (1973).
8. J. A. Manson and R. W. Hertzberg, *Crit. Rev. Macromol. Sci.,* **1,** 433 (1973).
9. H. R. Brown and I. M. Ward, *Polymer,* **14,** 469 (1973).
10. R. B. Taylor and A. V. Tobolsky, *J. Appl. Polym. Sci.,* **3,** 1563 (1964).
11. G. Rehage and W. Borchard, in *The Physics of Glassy Polymers,* R. N. Haward, Ed., Wiley, New York, 1973, Chap. 1, p. 54.
12. T. L. Smith, *J. Polym. Sci.,* **32,** 99 (1958).
13. T. L. Smith, *Rubber Chem. Technol.,* **41,** 1231 (1968).
14. J. C. Halpin, *J. Appl. Phys.,* **36,** 2975 (1965).
15. M. L. Williams, R. F. Landel, and J. D. Ferry, *J. Amer. Chem. Soc.,* **77,** 370 (1955).
16. J. L. Work and L. N. Ray, Jr., Lancaster, Pa., Armstrong Cork Co., 1969, unpublished report.
17. T. L. Smith, *Trans. Soc. Rheol.,* **6,** 61 (1962).
18. R. Sips, *J. Polym. Sci.,* **5,** 69 (1950).
19. T. L. Smith and R. A. Dickie, *J. Polym. Sci. A-2,* **7,** 635 (1969).
20. E. M. Smoley, unpublished data.
21. J. C. Halpin, *Rubber Chem. Technol.,* **38,** 1007 (1965).
22. R. N. Haward, in *The Physics of Glassy Polymers,* R. N. Haward, Ed., Wiley, New York, 1973, Chap. 6, p. 340.
23. J. A. C. Harwood, *J. Appl. Chem.,* **17,** 333 (1967).
24. A. Peterlin, in *Annual Review of Materials Science,* Vol. 2, R. A. Huggins, Ed., Palto Alto, Calif., Annual Rev. Inc., 1972, p. 349.

25. P. B. Bowden, in *The Physics of Glassy Polymers,* R. N. Haward, Ed., Wiley, New York, 1973, Chap. 5, p. 279.

26. T. L. Smith and J. E. Frederick, *J. Appl. Phys.,* **36,** 2996 (1965).

27. C. Bauwens-Crowet, J. C. Bauwens, and G. Homes, *J. Polym. Sci. A-2,* **7,** 235 (1969).

28. J. C. Bauwens, C. Bauwens-Crowet, and G. Homes, *J. Polym. Sci. A-2,* **7,** 1745 (1969).

29. G. S. Y. Yeh, *J. Macromol. Sci., Phys.,* **B7,** 729 (1973).

30. J. M. Kraft and H. L. Smith, Ligament Instability Model for Stress Corrosion and Fatigue Crack Propagation in a 4340 Steel, *NRL* Mem. Rep. 2598, April 1973.

31. J. G. Williams and C. E. Turner, *Appl. Mat. Res.,* 144 (July 1964).

32. N. G. McCrum, B. E. Read, and G. Williams, *Anelastic and Dielectric Effects in Polymeric Solids,* Wiley, New York, 1967, p. 428.

33. J. D. Ferry, *Viscoelastic Properties of Polymers,* Wiley, New York, 1961, p. 63.

Received February 21, 1975